HHS Public Access

Author manuscript

Mol Cell. Author manuscript; available in PMC 2019 October 18.

Published in final edited form as:

Mol Cell. 2018 October 18; 72(2): 211–221.e3. doi:10.1016/j.molcel.2018.08.031.

Impeding DNA Break Repair Enables Oocyte Quality Control

Huanyu Qiao[#1,2,†,*], **H.B.D. Prasada Rao**[#1,2,f], **Yan Yun**[1,2], **Sumit Sandhu**[1,2], **Jared H. Fong**[1,2], **Manali Sapre**[1,2], **Michael Nguyen**[1,2], **Addy Tham**[1,2], **Benjamin W. Van**[1,2], **Tiffany Y.H. Chng**[1,2], **Amy Lee**[1,2], and **Neil Hunter**[1,2,3,4,*]

[1]Howard Hughes Medical Institute, University of California, Davis, Davis, California, USA.

[2]Department of Microbiology & Molecular Genetics, University of California, Davis, Davis, California, USA.

[3]Department of Molecular & Cellular Biology, University of California, Davis, Davis, California, USA.

[4]Department of Cell Biology & Human Anatomy, University of California, Davis, Davis, California, USA.

[#] These authors contributed equally to this work.

SUMMARY

Oocyte quality control culls eggs with defects in meiosis. In mouse, oocyte death can be triggered by defects in chromosome synapsis and recombination, which involve repair of DNA double-strand breaks (DSBs) between homologous chromosomes. We show that RNF212, a SUMO ligase required for crossing over, also mediates oocyte quality control. Both physiological apoptosis and wholesale oocyte elimination in meiotic mutants require RNF212. RNF212 sensitizes oocytes to DSB-induced apoptosis within a narrow window as chromosomes desynapse and cells transition into quiescence. Analysis of DNA damage during this transition implies that RNF212 impedes DSB repair. Consistently, RNF212 is required for HORMAD1, a negative regulator of inter-sister recombination, to associate with desynapsing chromosomes. We infer that oocytes impede repair of residual DSBs to retain a “memory” of meiotic defects that enables quality control processes. These results define the logic of oocyte quality control and suggest RNF212 variants may influence transmission of defective genomes.

Graphical Abstract

[*]Correspondence to: Neil Hunter, nhunter@ucdavis.edu (lead contact) Huanyu Qiao, hqiao@illinois.edu.

AUTHOR CONTRIBUTIONS

H.Q., H.B.D.P.R. and N.H. conceived the study and designed the experiments. H.Q., H.B.D.P.R., F.H.F., M.S., M.N., A.T., B.W.V., T.Y-H.C. and A.L. performed the experiments and analyzed the data. S.S. advised and contributed to histological analysis. Y.Y. performed oocyte culture experiments. H.Q., H.B.D.P.R. and N.H. wrote the manuscript with inputs and edits from all authors.

[†]Current address: Comparative Biosciences, College of Veterinary Medicine, University of Illinois, Urbana, Illinois, USA.

[f]Current address: National Institute of Animal Biotechnology, Hyderabad, Telangana, India.

DECLARATION OF INTERESTS

The authors declare no competing interests.

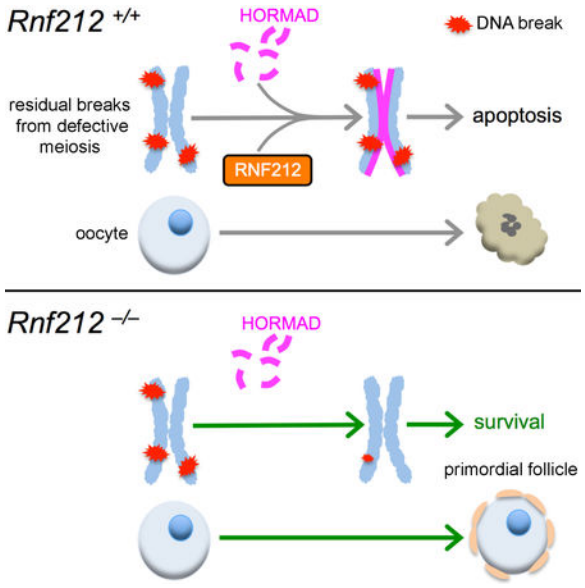

eTOC Blurb

High quality gametes (sperm and eggs) are paramount for successful reproduction. Defective gametes cause infertility and congenital disorders. Qiao et al. describe a counterintuitive process that helps developing eggs sense whether errors have occurred by impeding the repair of lingering chromosome breaks.

INTRODUCTION

Oocyte quality and number are important determinants of reproductive success (Kerr et al., 2013). These attributes are influenced by the selective elimination of oocytes that experience problems during the early stages of meiosis in a conserved process called fetal oocyte attrition (Bolcun-Filas et al., 2014; Cloutier et al., 2015; Di Giacomo et al., 2005; Hunter, 2017; Kerr et al., 2013; Kogo et al., 2012a; Malki et al., 2014; Rinaldi et al., 2017; Wojtasz et al., 2012). In mouse, epigenetic reprogramming during meiosis derepresses LINE-1 transposons triggering perinatal loss of at least half of all fetal oocytes (Malki et al., 2014). Defects in the chromosomal events of meiotic prophase also trigger oocyte loss, typically at a later stage than LINE-1 induced attrition, as oocytes transition into quiescence before developing into primordial follicles to establish the ovarian reserve (Di Giacomo et al., 2005; Hunter, 2017). This second wave of oocyte death is mediated by interrelated pathways that signal defective interactions between pairs of homologous chromosome, i.e. defects in DSB repair and/or homolog synapsis (Bolcun-Filas et al., 2014; Cloutier et al., 2015; Di Giacomo et al., 2005; Kogo et al., 2012a; Rinaldi et al., 2017; Wojtasz et al., 2012). Canonical DNA-damage response factors signal unrepaired DSBs via the ATR and CHK2 kinases to trigger p53/p63-mediated oocyte apoptosis. Defective synapsis can also trigger oocyte death by a distinct pathway that mediates transcriptional silencing in a process termed meiotic silencing of unpaired chromatin (MSUC). Together, these early and late oocyte attrition pathways balance the quality and size of the ovarian follicle reserve to maximize reproductive success. In this study, we address why and how defective

interhomolog interactions trigger oocyte apoptosis after chromosomes desynapse during the transition into quiescence. We implicate a new factor, RNF212, in the pre-follicle oocyte apoptosis pathway and show that it functions in a counterintuitive process that helps oocytes gauge whether meiotic inter-homolog interactions were defective.

RESULTS

Rnf212 Mutants Have Enlarged Oocyte Reserves

RNF212 is a RING-family E3-ligase that regulates the progression of meiotic recombination via the SUMO modification and ubiquitin-proteasome systems, and is essential for crossing over (Qiao et al., 2014; Rao et al., 2017; Reynolds et al., 2013). *Rnf212* mutation in mice causes sterility in both sexes. Although early events of meiotic prophase occur efficiently in *Rnf212*$^{-/-}$ mutants, including synapsis and DSB repair, crossing-over fails leaving homologs unconnected at metaphase I. In males, the resulting univalents are a potent trigger of apoptosis resulting in the complete absence of spermatids (Reynolds et al., 2013). Elimination of gametes was not seen in *Rnf212*$^{-/-}$ mutant females (Figure 1, A–E). On the contrary, large numbers of oocytes were present in *Rnf212*$^{-/-}$ mutant ovaries. This sexually dimorphic response to *Rnf212*$^{-/-}$ mutation presumably reflects the fact that postnatal oocytes are arrested in the dictyate stage, which follows crossing over and desynapsis of homologous chromosomes, but precedes the meiosis I division. Thus, the absence of crossovers in *Rnf212*$^{-/-}$ mutant oocytes goes undetected until they resume meiosis in the preovulatory stage of folliculogenesis, as seen for other mutants defective for late steps of crossing over (Hunter, 2017; Kan et al., 2008). Consistent with this interpretation, *in vitro* maturation experiments showed that oocytes from *Rnf212*$^{-/-}$ mutants resumed meiosis efficiently, but failed to successfully execute meiosis I (Figure S1). Thus, the absence of early defects in DSB repair and homolog synapsis allows non-fertile follicle reserves to be established in *Rnf212*$^{-/-}$ mutants.

Quantification of oocyte numbers revealed that oocyte reserves were significantly larger in *Rnf212*$^{-/-}$ mutants than in their wild-type counterparts. Ovaries dissected from 1, 4, 10 and 18 day old animals (day post-partum, dpp) were fixed, sectioned and immunostained for oocyte-specific markers (mouse vasa homologue, MVH; synaptonemal complex protein 3, SYCP3; and/or p63)(Figure 1, A–D, and Figure S2). At 1 and 4 days postpartum (dpp), oocyte numbers in *Rnf212*$^{-/-}$ mutant ovaries were indistinguishable from their wild-type counterparts (Figure 1E). However, the ovaries of 10 and 18 dpp *Rnf212*$^{-/-}$ mutants contained 45-57% more oocytes than wild-type ovaries.

RNF212 Promotes Physiological and Pathological Oocyte Apoptosis

One explanation for the larger oocyte pools of *Rnf212*$^{-/-}$ mutants is that RNF212 promotes oocyte apoptosis. To address this possibility, we immunostained early postnatal oocytes from 0.5, 1.0 and 2.0 dpp animals for the DNA-damage marker, phosphorylated histone H2AFX (γH2AX), and the apoptosis execution factor, Caspase 3 (Figure 1F and 1G). A subset of oocyte nuclei was identified with pan-nuclear staining for both γH2AX and Caspase 3, which is diagnostic of apoptotic nuclei (Harada et al., 2014) (Figure 1F). In wild-type animals, the fraction of apoptotic oocytes increased ~4-fold between 0.5 and 2.0 dpp (from 6

to 21%) indicating elevated apoptosis as oocytes transitioned into dictyate (Figure 1G). This increase was not seen in the *Rnf212*$^{-/-}$ mutant, for which levels of apoptotic nuclei remained low and relatively constant, at ~5% of total oocytes, between birth and 2 dpp. We conclude that RNF212 facilitates the apoptosis of a subset of early postnatal oocytes.

To test the idea that RNF212 promotes apoptosis of oocytes that have experienced errors in meiotic prophase I, we asked whether *Rnf212* mutation could rescue the wholesale elimination of oocytes caused by *Spo11* and *Msh4* mutations (Figure 2). *Spo11*$^{-/-}$ mutants fail to initiate meiotic recombination resulting in severely defective homolog synapsis and almost complete elimination of the oocyte pool (Figure 2A and 2C) (Baudat et al., 2000). Consistent with previous analysis (Di Giacomo et al., 2005), only a very small number of oocytes survived in *Spo11*$^{-/-}$ mutants at 18 dpp, less than 7.5% of wild type (Figure 2C and 1E). However, in *Spo11*$^{-/-}$ *Rnf212*$^{-/-}$ double mutants, large numbers of oocytes were present, averaging 40% of the oocyte numbers seen in *Rnf212*$^{-/-}$ single mutants (Figure 2B, 2C and 2G). More complete restoration of oocyte pools by *Rnf212* mutation was seen in the *Msh4*$^{-/-}$ mutant background. The absence of MSH4 causes severe defects in both DSB repair and homolog synapsis resulting in the complete elimination of oocytes within 4 days of birth (Kneitz et al., 2000)(Figure 2 D and 2F). Strikingly, the ovaries of *Msh4*$^{-/-}$ *Rnf212*$^{-/-}$ double mutants contained high numbers of oocytes, averaging 75% of those in the *Rnf212*$^{-/-}$ single mutant (Figure 2E, 2F and 2G). Moreover, small numbers of oocytes were able to escape apoptosis even when the *Rnf212* mutation was heterozygous in the *Msh4*$^{-/-}$ background (Figure S3). Thus, the complete elimination of oocytes in *Msh4*$^{-/-}$ mutants is sensitive to the level of RNF212.

RNF212 Modulates DNA Damage Levels in Early Postnatal Oocytes

The data above indicate that RNF212 promotes apoptosis of oocytes that have experienced defects in meiotic prophase I. RNF212 could influence the primary signaling of defects in recombination and synapsis, for example by altering DSB repair. Alternatively, RNF212 could be a component of downstream signaling pathways that ultimately trigger apoptosis. To distinguish these possibilities, we monitored levels of DNA damage in early postnatal oocyte nuclei via γH2AX immunostaining (Figure 3A and 3B). During meiosis, γH2AX decorates the chromatin around DSBs and accumulates at regions of chromosomes that fail to undergo synapsis (Cloutier et al., 2015; Mahadevaiah et al., 2001). We reasoned that if RNF212 functions solely in downstream steps to signal damage or trigger apoptosis, presumptively defective oocytes with high levels of γH2AX should be present at highly elevated levels in the ovaries of *Rnf212*$^{-/-}$ mutants. Oocytes from 1 dpp mice were found to be in one of three stages: late pachytene, diplotene or early dictyate (Figure 3A). In late pachytene nuclei, an average of 40 ± 15 γH2AX chromatin “flares” were detected, decreasing to 21 ± 11 in diplotene, and just 6 ± 3 as oocytes transitioned into dictyate (Figure 3A and 3B). Contrary to expectations, numbers of γH2AX flares were ~2-fold lower at all stages in the early postnatal oocytes of *Rnf212*$^{-/-}$ mutants implying lower DSB levels. *Rnf212*$^{-/-}$ oocytes entering dictyate contained an average of only 2.7 ± 1.4 γH2AX flares, compared to 6 ± 3 in wild-type cells; moreover, 20% of nuclei had no staining at all, compared to just 6% of wild-type oocytes (Figure 3A and 3B). Qualitatively, the γH2AX

signals detected in *Rnf212*$^{-/-}$ oocytes were generally fainter and more compact than those seen in wild type.

Given that γH2AX can mark both DSBs and non-DSB lesions during meiosis (Cloutier et al., 2015), we also immunostained oocytes from 1 dpp animals for Replication Protein A (RPA), which tightly binds regions of single-stranded DNA created during replication, repair and recombination (Ribeiro et al., 2016)(Figure 3C and 3D). RPA-staining foci were detected in similar numbers to γH2AX flares, suggesting that the vast majority of γH2AX signals in wild-type and *Rnf212*$^{-/-}$ oocytes mark sites of DNA lesions, very likely DSBs. Moreover, like γH2AX flares, numbers of RPA foci were reduced ~2-fold in *Rnf212*$^{-/-}$ mutant oocytes.

Together, these data imply that RNF212 modulates the generation or processing of DNA damage that leads to oocyte apoptosis. To distinguish these possibilities, the processing of exogenous DNA damage was examined by exposing 1 dpp wild-type and *Rnf212*$^{-/-}$ animals to 1 Gy γ-irradiation, estimated to inflict ~20 DSBs per nucleus (Figure 3E)(Rinaldi et al., 2017; Suh et al., 2006). Post-irradiation γH2AX signals were then quantified in diplotene and early dictyate nuclei after 2 and 24 hours (Figure 3F–H). After 2 hrs, wild-type nuclei had developed pan-nuclear γH2AX chromatin staining signals reflecting extensive DNA damage. In stark contrast, only axis-associated γH2AX flares and puncta were observed in *Rnf212*$^{-/-}$ oocytes, similar to those seen in unirradiated oocytes, and total γH2AX staining areas were reduced at least 2-fold relative to wild type (Figure 3A). At 24 hrs, pan-nuclear staining persisted in wild-type oocytes and γH2AX staining areas were indistinguishable from those at 2 hrs (P=0.53, unpaired t-test) indicating unrepaired damage. In *Rnf212*$^{-/-}$ oocytes, γH2AX staining areas at 24 hrs were significantly reduced relative to 2 hrs (P=0.024, unpaired t-test) and residual γH2AX signals comprised mostly very small foci, some clustered and some dispersed, many of which were not axis associated (Figure 3G). Thus, the processing of radiation-induced DNA damage differs dramatically in wild-type and *Rnf212*$^{-/-}$ mutant oocytes, with much more efficient and rapid repair occurring in the latter.

RNF212 Impedes DNA Damage Repair in Meiotic Mutants

The inference that RNF212 impedes DSB repair in early postnatal oocytes was further explored by quantifying DNA-damage markers in oocytes from the meiotic mutants, *Spo11*$^{-/-}$ and *Msh4*$^{-/-}$, and the corresponding double mutants with *Rnf212*$^{-/-}$ (Figure 4 and Figure S4). The defective homolog synapsis that occurs in *Spo11*$^{-/-}$ and *Msh4*$^{-/-}$ mutants makes it hard to distinguish oocytes in late pachytene from those in diplotene. Therefore, we could assign only two categories of oocyte nuclei in these mutants: “early” nuclei had bright, contiguous SYCP3-staining axes and were inferred to be in pachytene- and diplotene-like stages; and “late” nuclei had fainter, fragmented SYCP3 axes and were inferred to be either early dictyate or early apoptotic oocytes (Figure 4A). In early-stage *Spo11*$^{-/-}$ oocytes from 1 dpp animals, γH2AX staining was present as numerous large flares, encompassing long portions of individual chromosome axes indicative of the extensive transcriptional silencing that occurs in response to asynapsis called meiotic silencing of unpaired chromatin (MSUC) (Baarends et al., 2005; Cloutier et al., 2015; Kouznetsova et al., 2009; Turner et al., 2005).

88% of *Spo11*$^{-/-}$ oocytes showed this pattern, while 12% had pan-nuclear staining (Figure 4A, 4B and 4C, and Figure S4). Much more extensive γH2AX staining was seen in late-stage *Spo11*$^{-/-}$ mutant oocytes; more than 91% showed pan-nuclear staining, while the remainder had a pattern of extended γH2AX flares. Mutation of *Rnf212*$^{-/-}$ in the *Spo11*$^{-/-}$ background greatly reduced the extent of γH2AX staining. In late-stage *Rnf212*$^{-/-}$ *Spo11*$^{-/-}$ oocytes, the fraction of nuclei with pan-nuclear staining was reduced by half (45% versus 91% in the *Spo11*$^{-/-}$ single mutant) with a corresponding increase in nuclei with γH2AX flares. Moreover, for both early and late-stage *Rnf2l2*$^{-/-}$ *Spo11*$^{-/-}$ oocytes containing γH2AX flares, the total staining areas were greatly reduced, by 5-fold, relative to those of nuclei from the *Spo11*$^{-/-}$ single mutant (Figure 4E and Figure S4). *Rnf2l2* mutation also diminished γH2AX signals in *Msh4*$^{-/-}$ mutant oocytes, but the effects were more extreme (Figure 4A, 4B and 4C, and Figure S4). 85% of early-stage and 91% of late-stage oocytes from the *Msh4*$^{-/-}$ mutant showed pan-nuclear γH2AX staining. Oppositely, ~80% of oocytes from *Rnf2l2*$^{-/-}$ *Msh4*$^{-/-}$ double mutants had the γH2AX flare-staining pattern, with greatly reduced (30-fold) staining areas compared to those of *Msh4*$^{-/-}$ single mutant nuclei. Thus, *Rnf2l2* mutation diminishes the very high levels of γH2AX that occur in early postnatal oocytes of both *Spo11*$^{-/-}$ and *Msh4*$^{-/-}$ mutants.

Supporting the interpretation that *Rnf2l2* mutation is reducing the level of DNA damage present in early postnatal oocytes of *Spo11*$^{-/-}$ and *Msh4*$^{-/-}$ mutants, RPA foci showed changes similar to those seen for γH2AX (Figure 4D and 4E). In *Spo11*$^{-/-}$ and *Msh4*$^{-/-}$ single mutants, early-stage oocytes contained an average of 50 ± 53 and 77 ± 42 RPA foci, respectively. The presence of high levels of Spo11-independent DSBs in *Spo11*$^{-/-}$ mutant oocytes was previously documented and shown to make a significant contribution to oocyte apoptosis in this asynaptic background via the DNA damage response (Carofiglio et al., 2013; Carofiglio et al., 2018; Rinaldi et al., 2017). Although the origin of these breaks is currently unknown, a likely source is LINE-1 activity (Malki et al., 2014). In contrast to wild-type animals, in which RPA focus numbers decreased as oocytes transitioned into dictyate (Figure 3C and 3D), foci further increased in late-stage *Spo11*$^{-/-}$ and *Msh4*$^{-/-}$oocytes (Figure 4D and 4E), mirroring the transition to pan-nuclear γH2AX staining in these mutants (Figure 4A and 4B). *Rnf212*$^{-/-}$ mutation decreased RPA focus numbers by 3 to 4 fold in both *Spo11*$^{-/-}$ and *Msh* backgrounds. Thus, consistent with the idea that RNF212 impedes DSB repair in early postnatal oocytes, the presence of RNF212 greatly enhances DNA damage levels in meiotic mutants defective for homolog synapsis and DSB repair.

RNF212 is Required for HORMAD1 to Associate With Desynapsing Chromosomes as Oocytes Transition into Quiescence

The ability of *Rnf212* mutation to suppress the oocyte death of recombination and synapsis mutants is shared by mutation of the *Hormad1* gene that encodes a meiosis-specific HORMA (Hop1, Rev7 and Mad2)-domain protein with central roles in regulating the events of meiotic prophase I (Daniel et al., 2011; Kogo et al., 2012b; Shin et al., 2013). HORMAD1 and its orthologs have been implicated in meiotic DSB formation, homolog pairing and synapsis, checkpoint signaling, transcriptional silencing (MSUC), and biasing meiotic recombination to occur between homologs by impeding inter-sister DSB repair

(Carballo et al., 2008; Rinaldi et al., 2017; Royo et al., 2013; Shin et al., 2010; Stanzione et al., 2016; Vader and Musacchio, 2014). HORMAD1 is initially associated with unsynapsed chromosome axes during early prophase I, but then becomes depleted as homologs synapse, before re-associating with desynapsing axes during diplonema (Fukuda et al.; Niu et al., 2005; Wojtasz et al., 2009)(Figure 5A).

The role of HORMAD1 upon its reassociation with desynapsed diplotene chromosomes is unknown, but its timing and location suggest the potential to influence the repair of residual DSBs between sister chromatids. Therefore, we asked whether *Rnf212* mutation affects the reassociation of HORMAD1 with diplotene and early dictyate chromosomes (Figure 5A). Immunostaining of oocyte chromosome spreads from 1 dpp wild-type animals revealed strong association of HORMAD1 with desynapsed homolog axes in early diplotene nuclei (Figure 5A, top row). In nuclei where desynapsis was more advanced, extensive association of HORMAD1 was seen along the lengths of all desynapsed axes. This extensive HORMAD1 staining pattern persisted into early dictyate, even in nuclei where the SYCP3-staining axes had become faint and highly fragmented. In $Rnf212^{-/-}$ mutant oocytes, association of HORMAD1 with diplotene and dictyate chromosomes was greatly diminished (Figure 5A, bottom row). To quantify this defect, we binned nuclei into three HORMAD1 staining-classes based on their relative signal intensities (Figure 5C and Figure S5). In wild-type nuclei from 1 dpp animals, 61, 23 and 16% of nuclei showed high, medium and low intensity HORMAD1 staining, respectively; compared to 20, 47 and 33% of $Rnf212^{-/-}$ mutant nuclei ($P<0.001$, G-test). We also examined HORMAD1 dynamics in 1 dpp $Msh4^{-/-}$ mutants, in which all oocytes are destined for apoptosis, and in $Rnf212^{-/-}$ $Msh4^{-/-}$ double mutants where most oocytes survive (Figure 5B and 5C). High-intensity HORMAD1 staining was observed in 85% of $Msh4^{-/-}$ oocyte nuclei (both early and late stage nuclei, defined by the criteria described above). Again, chromosomal association of HORMAD1 was greatly diminished by $Rnf212^{-/-}$ mutation; just 24% of nuclei from $Rnf212^{-/-}$ $Msh4^{-/-}$ double mutants showed high intensity HORMAD1 staining ($P<0.001$, G-test). Thus, RNF212 promotes or stabilizes the association of HORMAD1 along desynapsed homolog axes both in wild-type oocytes and in mutants such as $Msh4^{-/-}$that experience severe defects in synapsis and recombination.

RNF212 Enhances DSB-Induced Apoptosis as Oocytes Transition into Quiescence

The data above suggest that the transition into quiescence, from the diplotene to dictyate stages, marks a critical oocyte quality-control juncture where the success of meiotic prophase is determined by assessing levels of residual DNA damage. To test this interpretation we asked if exogenous DSBs, inflicted specifically during the early postnatal period, could trigger oocyte apoptosis and whether RNF212 enhanced this process (Figure 6). Animals were exposed to γ-irradiation at different times during the two-day window after birth when oocytes transition into dictyate. Previous studies showed that exposure of 5 dpp mice to 0.45 Gy, estimated to induce ~10 DSBs per nucleus, efficiently triggered apoptosis (Rinaldi et al., 2017; Suh et al., 2006). Therefore, we initially exposed wild-type and $Rnf212^{-/-}$ littermates, at 0.5, 1 or 2 dpp, to 0.45 Gy. Oocyte numbers from irradiated mice were then quantified at 10 dpp and compared to unirradiated controls (Figure 5A-D). At 0.5 dpp, oocytes were largely resistant to radiation-induced apoptosis. Oocyte numbers in

both wild-type and *Rnf212*$^{-/-}$ animals were similar to those of unirradiated wild-type controls $P > 0.58$; Figure 6D), but still smaller than those of unirradiated *Rnf212*$^{-/-}$ animals. In contrast, oocytes at 1 and 2 dpp were highly sensitive to radiation-induced apoptosis. Survival of wild-type oocytes averaged only 16% and 7% of unirradiated controls following exposure to 0.45 Gy at 1 and 2 dpp, respectively (Figure 6D). Survival of *Rnf212*$^{-/-}$ oocytes irradiated at 1 and 2 dpp was slightly higher than wild type, averaging respectively 21% and 10% of the *Rnf212*$^{-/-}$ mutant unirradiated controls (or 39% and 20% of wild-type unirradiated controls). Thus, at 0.5 dpp, both wild-type and *Rnf212* oocytes are largely resistant to a dose of irradiation that becomes a potent trigger of apoptosis at 1 and 2 dpp, as oocytes transition into dictyate.

Suh et al. (Suh et al., 2006) demonstrated a narrow dose-response relationship between γ-irradiation and oocyte apoptosis. This fact, together with the suggestion that *Rnf212*$^{-/-}$ mutant oocytes are slightly more resistant to 0.45 Gy at 1 and 2 dpp (Figure 6D), motivated us to examine the effects of a lower dose of irradiation (Figure 6E–G). With a dose of 0.35 Gy (equivalent to ~7 DSBs per nucleus), both wild-type and *Rnf212*$^{-/-}$ oocytes were again largely resistant to apoptosis when exposed at 0.5 dpp, but highly sensitive when exposed at 2 dpp, similar to the responses observed with 0.45 Gy. However, a striking difference in sensitivity was observed when mice were exposed at 1 dpp. While wild-type oocytes remained highly sensitive, averaging only 13% survival (relative to unirradiated wild type), *Rnf212*$^{-/-}$ mutant oocytes were largely resistant with 68% survival relative to unirradiated *Rnf212*$^{-/-}$ controls (Figure 6G). We conclude that RNF212 enhances DSB-induced apoptosis during a narrow window as oocytes transition from diplotene to dictyate.

DISCUSSION

Together, our data delineate a major oocyte quality control point at the diplotene-to-dictyate transition during which DSB repair is actively impeded in order to gauge whether the events of early meiotic prophase occurred successfully (Figure 7). At this stage, an unrepaired DSB is indicative of a failed inter-homolog interaction, or possibly a lesion resulting from LINE-1 activity (Malki et al., 2014). During diplotene, homologs are no longer closely juxtaposed (except very locally at crossover sites) and inter-homolog recombination factors are no longer present such that accurate repair of residual DSBs can only be achieved via recombination with the sister chromatid. By blocking inter-sister recombination, RNF212-dependent re-loading of HORMAD1 onto desynapsed homolog axes effectively acts to preserve a “memory” of meiotic prophase errors. Reinstallation of HORMAD1 could similarly impede repair of residual LINE-1 induced damage, and also reinforce transcriptional silencing via MSUC, which requires HORMAD proteins (Royo et al., 2013; Wojtasz et al., 2012). Consequently, a robust signaling response from any residual lesions will be maintained during the diplotene-to-dictyate transition enabling a meiotic quality-control decision to be made (Figure 7). Signaling above a critical threshold efficiently triggers apoptosis thereby preventing oocytes that have experienced significant recombination and synapsis errors, or high levels of LINE-1 activity, from contributing to the ovarian reserve. Consistent with the study of Rinaldi et al. (2017), we estimate that this threshold is equivalent to ~10 DSBs per nucleus (Figure 6). Importantly, our data indicate that pre-follicle apoptosis is a significant physiological quality-control pathway that removes

as much as half of the oocytes that remain after LINE-1 induced early oocyte attrition (Malki et al., 2014). Together, we can estimate that fetal and pre-follicle attrition cull ~75% of all oocytes in mouse (Malki et al., 2014)(this study), mirroring the dramatic reduction in oocyte numbers seen in human females between ~20 weeks gestation and birth (Findlay et al., 2015), presumably via equivalent quality control mechanisms.

Analysis of recombination intermediates in budding yeast has provided direct evidence that Hop1^{HORMAD} negatively regulates inter-sister recombination as part of a phospho-kinase signal-transduction pathway that responds to DSBs (Humphryes and Hochwagen, 2014; Lao and Hunter, 2010). Following DSB-dependent phosphorylation by PI3K-like sensor kinases, Mec1^{ATR} and Tel1^{ATM}, Hop1^{HORMAD} acts as a mediator for activation of the effector kinase, Mek1, which directly targets components of the recombination and cell-cycle machinery (Callender et al., 2016; Carballo et al., 2008; Prugar et al., 2017). Two lines of evidence in mouse indicate that mammalian HORMADs also negatively regulate inter-sister recombination; first, repair of irradiation-induced DSBs is accelerated when HORMADs are absent; and second, DSB levels are diminished in asynaptic *Spo11*$^{-/-}$ mutant meiocytes in which inter-sister recombination is likely the only repair option (Carofiglio et al., 2018; Rinaldi et al., 2017; Shin et al., 2013).

HORMAD1 initially loads onto leptotene chromosomes independently of RNF212 (data not shown). After homolog pairing has been achieved, we propose that nascent interhomolog interactions are “locked in” by synaptonemal complexes and associated meiosis-specific recombination factors (ZMMs)(Hunter, 2015; Lynn et al., 2007). Consequently, the role of HORMAD proteins in preventing intersister recombination is no longer necessary. Indeed, dissociation of HORMADs as synapsis ensues may enable inter-sister repair of DSBs that either failed to engage a homolog template, or that engaged in interhomolog DNA strand exchange to facilitate pairing, but did not complete repair. Estimates of unrepaired DSB numbers in the *Trip13* mutant, which fails to remove HORMADs from homolog axes upon synapsis, implies that up to a quarter of DSBs may utilize inter-sister recombination for their repair (Rinaldi et al., 2017). Our observation that late pachytene cells are relatively insensitive to DSB-induced apoptosis (Figure 6)(Hanoux et al., 2007) could be explained, at least in part, by a larger capacity to repair DSBs via inter-sister recombination following the dissociation of HORMAD proteins. As such, many more DSBs would be required to reach the signaling threshold required to induce apoptosis at this stage. In addition, the signaling threshold required to induce apoptosis during pachytene may be increased in order to prevent aberrant culling of oocytes that are still completing recombination (Hanoux et al., 2007; Kim and Suh, 2014). The window in which RNF212 enhances DSB-induced apoptosis also likely reflects the timing of expression of the transactivating p63 isoform, TAp63, and components of the apoptotic machinery. As oocytes progress into dictyate, TAp63, becomes fully expressed and activatable by phosphorylation rendering primordial follicles exquisitely sensitive to DNA damage (Kim and Suh, 2014; Livera et al., 2008; Suh et al., 2006). Similarly, expression of the initiator caspase, caspase-2, correlates with the onset of radiosensitivity in early postpartum oocytes (Hanoux et al., 2007).

RNF212 is known for its essential role in meiotic crossing over (Qiao et al., 2014; Rao et al., 2017; Reynolds et al., 2013). At the cytological level, RNF212 promotes chromosome-

associated SUMO conjugation during early meiotic prophase and renders the progression of recombination beyond nascent strand-exchange intermediates dependent on the action of the ubiquitin-proteasome system, mediated specifically by a second RING ligase, HEI10. RNF212 initially localizes as numerous puncta along synapsed chromosomes during zygotene and early pachytene, before accumulating specifically at future crossover sites (Reynolds et al., 2013). However, RNF212 is not detected along desynapsing chromosomes during diplotene, i.e. during the time it ostensibly mediates the reassociation of HORMAD1. This observation suggests that RNF212 may function in the nucleoplasm to license HORMAD1 to reassociate with homolog axes upon desynapsis. Alternatively, such a licensing step could occur much earlier, in early-mid pachytene when RNF212 localizes along synaptonemal complexes, but HORMAD1 loading would be contingent upon subsequent desynapsis. Possibly, RNF212 prevents HORMAD1 from being degraded and/or antagonizes the action of TRIP13, an AAA+ ATPase required to dissociate HORMADs from synapsed homolog axes (Li and Schimenti, 2007; Roig et al., 2010; Wojtasz et al., 2009; Ye et al., 2017). Given that low levels of chromosome-associated HORAMD1 are still detected in *Rnf212* mutant oocytes during diplotene and dictyate (Figure 5), RNF212 may primarily affect the ability of HORMAD1 to oligomerize, a fundamental attribute of HORMAD proteins that is central to their function (Kim et al., 2014; Rosenberg and Corbett, 2015; Ye et al., 2017).

Like yeast Hop1, HORMAD1 is important for DSB formation. Thus *Hormad1* mutant phenotypes reflect both reduced DSBs and derepression of inter-sister recombination (Daniel et al., 2011; Shin et al., 2010). *Rnf212* mutation does not impact the early roles of HORMAD1 in DSB formation and inter-homolog bias (Reynolds et al., 2013), but reveals a previously undefined late role as it reassociates with diplotene chromosome axes. This unanticipated role of RNF212 implicates SUMO modification in oocyte quality control and suggests that common variants of mammalian *Rnf212* genes (Johnston et al., 2016; Kadri et al., 2016; Kong et al., 2008) could have compound effects on crossing over, and the size and quality of oocyte reserves.

STAR METHODS

METHODS CONTACT FOR REAGENT AND RESOURCE SHARING

Further information and requests for resources and reagents should be directed to and will be fulfilled by the Lead Contact Neil Hunter, nhunter@ucdavis.edu

EXPERIMENTAL MODEL AND SUBJECT DETAILS

The oocytes analyzed in this study come from female fetuses at 18 days postcoitum (dpc) and from pups at 0.5, 1, 2, 4, 10, and 18 days postpartum (dpp). All mice were congenic with the C57BL/6J background. The *Rnf212*$^{-/-}$, *Msh4*$^{--}$, and *Spo11*$^{-/-}$ lines were previously described (Baudat et al., 2000; Kneitz et al., 2000; Reynolds et al., 2013). Mice were maintained and used for experimentation according to the guidelines of the Institutional Animal Care and Use Committees of the University of California, Davis. Mice were housed under 12 hour dark, 12 hour light cycles and fed *ad libitum* with regular chow.

QUANTIFICATION AND STATISTICAL ANALYSIS

Most data are presented as means ± SEM or SD and represent at least three independent experiments. Statistical tests, *P* and *n* values are described in the figures and figure legends.

METHODS DETAILS

Ovary Processing and Staining—Ovaries were dissected from freshly euthanized animals at the indicated ages and fixed in 10% formalin overnight. After washing in 70% ethanol, ovaries were embedded in paraffin and sectioned onto glass slides (5 μm sections for ovaries from 1 and 4 dpp animals; 8 μm sections for mice older than 4 dpp). Sections were then deparaffinized, rehydrated and incubated with antigen retrieval buffer (10 mM Sodium Citrate, 0.05% Tween-20) for 50 minutes at 100°C. Slides were blocked in serum free blocking solution (Dako X0909) for one hour followed by Antibody Dilution Buffer (10% normal goat serum, 3% BSA, 0.05% Triton X-100, 0.05% sodium azide) for 15 minutes at room temperature. Incubation with primary antibodies was performed overnight at room temperature. Ovaries from 1 and 4 dpp mice were stained for immunofluorescence using mouse anti-p63 (Santa Cruz Biotechnology, sc-25268; 1:500 dilution) antibodies, rabbit anti-MVH (Abcam, ab13840; 1:500) and/or rabbit anti-SYCP3 (Santa Cruz Biotechnology, sc-33195; 1:300 dilution) antibodies. Slides were subsequently incubated with one of two pairs of goat secondary antibodies for 1 h at 37°C: (1) anti-rabbit 488 (Molecular Probes, A11070; 1:1,000 dilution) and anti-mouse 594 (Molecular Probes, A11020; 1:1,000 dilution); or (2) anti-rabbit 568 (Molecular Probes, A11036; 1:1,000 dilution) and anti-mouse 488 (A11029 Molecular Probes, 1:1000). Ovaries from mice older than 4 dpp were stained for immunohistochemistry (IHC) with anti-p63 antibody (Santa Cruz Biotechnology, sc-25268; 1:500 dilution) overnight at room temperature. Biotin-conjugated anti-mouse secondary antibody (ThermoFisher Scientific, A16076; 1:1000 dilution) was used at a 1:1000 dilution for 1 h at 37°C. IHC signals were developed with the ABC-DAB Peroxidase system (Vector Labs), counterstained with hematoxylin for 10 seconds, and mounted with Permount solution.

Irradiation—At the indicated ages, mice received a single dose of ionizing radiation (0.35 or 0.45 Gy) on a rotating turntable in a ^{137}Cs irradiator (dose rate 9.8 rad min^{-1}). Irradiated mice and non-irradiated controls were euthanized at 10 dpp and their ovaries harvested and processed for oocyte quantification as described above.

Oocyte culture and metaphase I chromosome spreads—Germinal-vesicle stage oocytes were collected from mature mice (2-4 months old) without prior hormonal stimulation. Only oocytes with integral cumulus cell layers were used. 20-30 oocytes were collected per mouse. Surrounding cumulus cells were mechanically removed for observation of Germinal Vesicle Breakdown (GVBD) and Polar Body Extrusion (PBE). Oocytes were manipulated in M2 medium containing 2.5 μM milrinone (Sigma-Aldrich) under mineral oil at 37°C and maturation was stimulated by milrinone washout (Yun et al., 2014). GVBD was scored every 20 minutes by manual inspection over the first 2 hours and then scored again after 3 hours. Only oocytes that underwent GVBD within 3 hours were used to quantify PBE after 15 hours of incubation. All incubation times were relative to milrinone washout. To count chiasmata, oocytes were cultured in M2 media for 7 h, and then prepared for

metaphase-I chromosome spreads (Chambon et al., 2013). Acid Tyrode's solution (Sigma-Aldrich) was applied to remove zona pellucida, and zona-free oocytes were spread in 1% paraformaldehyde plus 0.15% Triton-X-100. DNA was stained with DAPI and centromeres were immunostained with human anti-centromere antibodies (ACA; HCT-0100 ImmunoVision, 1:1000 dilution) overnight at room temperature, followed by anti-human 555 (Molecular Probes, 1: 1000 dilution) secondary antibody for 1 h at 37°C.

Oocyte nuclei spreads and immunofluorescence cytology—Ovaries were dissected from freshly euthanized animals and processed for surface spreading of oocyte chromosomes as described (Sun and Cohen, 2013). Immunofluorescence staining was performed using the following primary antibodies with incubation overnight at room temperature: mouse anti-SYCP3 (sc-74568 Santa Cruz, 1:200 dilution), rabbit anti-SYCP3 (sc-33195 Santa Cruz, 1:300), guinea pig anti-SYCP2 (a gift from Christer Höög, 1:300) (Kouznetsova et al., 2005), rabbit monoclonal anti-RPA32 (ab76420 Abcam, 1:100), rabbit anti-REC8 (a gift from Scott Keeney, 1:300), mouse monoclonal anti-γH2AX (05-636 Millipore, 1:500), rabbit polyclonal anti-γH2AX (A300-081A Bethyl laboratories, 1:300), goat polyclonal anti-Caspase3 (L-18 Sc-1225, 1:100), rabbit anti-HORMAD1 (a gift from Attila Toth, 1:250)(Wojtasz et al., 2009). Slides were subsequently incubated with the following goat secondary antibodies for 1 h at 37 °C: anti-rabbit 488 (A11070 Molecular Probes, 1:1000 dilution), anti-rabbit 568 (A11036 Molecular Probes, 1:2000), anti-mouse 555 (A21425 Molecular Probes, 1:1000), anti-mouse 594 (A11020 Molecular Probes, 1:1000), anti-mouse 488 (A11029 Molecular Probes, 1: 1000), or anti-guinea pig fluorescein isothiocyanate (106-096-006 FITC, Jackson Labs, 1:200). Coverslips were mounted with ProLong Gold antifade reagent (Molecular Probes).

Quantification and Statistical Analysis—Immunofluorescence-stained ovary sections and chromosome spreads were imaged using a Zeiss AxioPlan II microscope with a 20× Plan Apochromat 0.45 NA, or 63× Plan Apochromat 1.4 NA objective and EXFO X-Cite metal halide light source. Images were captured with a Hamamatsu ORCA-ER CCD camera and processed using Volocity software (Perkin Elmer). Immunohistochemistry-stained ovary sections were imaged using a ScanScope digital scanner (Aperio) and processed using ImageScope software. All comparisons were made between datasets obtained from animals that were either littermates, or matched by age. Two observers performed all quantitative analyses; the second observer was blind to which group/genotype was being analyzed. For immunofluorescence-stained ovary sections, MVH/SYCP3-positive oocytes with or without p63 stained nuclei were counted. For immunohistochemistry-stained ovary sections, p63-positive oocyte nuclei with characteristic surrounding granulosa cell layers were counted. In both cases, counts were made for every fifth section, as described (Di Giacomo et al., 2005). Counts were multiplied by five to calculate the total number of oocytes per ovary. Control counts for every ovary section confirmed the accuracy of this approach. For each genotype or condition, 3-8 ovaries were analyzed. For quantifications of spread oocyte nuclei, images of 90-160 nuclei from at least two animals were analyzed. SYCP3-staining nuclei were staged using standard criteria. In late pachytene, homologs are still fully synapsed and SYCP3 is present as 20 contiguous lines; during diplotene homologs desynapse and SYCP3 lines split; and as cells enter dictyate SYCP3 lines begin to dissolve and fragment, and are

often accompanied by bright aggregates of SYCP3. To quantify high-density γH2AX and HORMAD1 signals, intensity ratios were calculated: total signal for γH2AX or HORMAD1 was divided by the total signal for SYCP3.

A. Data and Software Availability

B. Additional Resources

N/A

Supplementary Material

Refer to Web version on PubMed Central for supplementary material.

ACKNOWLEDGMENTS

We thank Supipi Mirihagalle for help with oocytes counts, Richard Shultz for advice and support; Vera Rinaldi, Ewilina Bolcun-Filas and John Schimenti for discussions and sharing unpublished data; Attila Toth, Christer Höög and Scott Keeney for antibodies; Jim Trimmer for ScanScope access; Shanie McCarty for assistance with irradiation experiments; and the Hunter Lab for support and discussions. H.Q. was supported by NICHD Pathway to Independence Award K99/R00HD082375. S.S. was supported by the A.P. Giannini Foundation. This work was initially supported by NIGMS grant GM084955. N.H. is an Investigator of the Howard Hughes Medical Institute.

REFERENCES

Baarends WM, Wassenaar E, van der Laan R, Hoogerbrugge J, Sleddens-Linkels E, Hoeijmakers JH, de Boer P, and Grootegoed JA (2005). Silencing of unpaired chromatin and histone H2A ubiquitination in mammalian meiosis. Molecular and cellular biology 25, 1041–1053. [PubMed: 15657431]

Baudat F, Manova K, Yuen JP, Jasin M, and Keeney S (2000). Chromosome synapsis defects and sexually dimorphic meiotic progression in mice lacking Spo11. Molecular cell 6, 989–998. [PubMed: 11106739]

Bolcun-Filas E, Rinaldi VD, White ME, and Schimenti JC (2014). Reversal of female infertility by Chk2 ablation reveals the oocyte DNA damage checkpoint pathway. Science 343, 533–536. [PubMed: 24482479]

Callender TL, Laureau R, Wan L, Chen X, Sandhu R, Laljee S, Zhou S, Suhandynata RT, Prugar E, Gaines WA, et al. (2016). Mek1 Down Regulates Rad51 Activity during Yeast Meiosis by Phosphorylation of Hed1. PLoS genetics 12, e1006226. [PubMed: 27483004]

Carballo JA, Johnson AL, Sedgwick SG, and Cha RS (2008). Phosphorylation of the axial element protein Hop1 by Mec1/Tel1 ensures meiotic interhomolog recombination. Cell 132, 758–770. [PubMed: 18329363]

Carofiglio F, Inagaki A, de Vries S, Wassenaar E, Schoenmakers S, Vermeulen C, van Cappellen WA, Sleddens-Linkels E, Grootegoed JA, Te Riele HP, et al. (2013). SPO11-independent DNA repair foci and their role in meiotic silencing. PLoS genetics 9, e1003538. [PubMed: 23754961]

Carofiglio F, Sleddens-Linkels E, Wassenaar E, Inagaki A, van Cappellen WA, Grootegoed JA, Toth A, and Baarends WM (2018). Repair of exogenous DNA double-strand breaks promotes chromosome synapsis in SPO11-mutant mouse meiocytes, and is altered in the absence of HORMAD1. DNA repair 63, 25–38. [PubMed: 29414051]

Chambon JP, Hached K, and Wassmann K (2013). Chromosome spreads with centromere staining in mouse oocytes. Methods in molecular biology 957, 203–212. [PubMed: 23138954]

Cloutier JM, Mahadevaiah SK, ElInati E, Nussenzweig A, Toth A, and Turner JM (2015). Histone H2AFX Links Meiotic Chromosome Asynapsis to Prophase I Oocyte Loss in Mammals. PLoS genetics 11, e1005462. [PubMed: 26509888]

Daniel K, Lange J, Hached K, Fu J, Anastassiadis K, Roig I, Cooke HJ, Stewart AF, Wassmann K, Jasin M, et al. (2011). Meiotic homologue alignment and its quality surveillance are controlled by mouse HORMAD1. Nature cell biology 13, 599–610. [PubMed: 21478856]

Di Giacomo M, Barchi M, Baudat F, Edelmann W, Keeney S, and Jasin M (2005). Distinct DNA-damage-dependent and -independent responses drive the loss of oocytes in recombination-defective mouse mutants. Proceedings of the National Academy of Sciences of the United States of America 102, 737–742. [PubMed: 15640358]

Findlay JK, Hutt KJ, Hickey M, and Anderson RA (2015). How Is the Number of Primordial Follicles in the Ovarian Reserve Established? Biology of reproduction 93, 111. [PubMed: 26423124]

Fukuda T, Daniel K, Wojtasz L, Toth A, and Hoog C A novel mammalian HORMA domain-containing protein, HORMAD1, preferentially associates with unsynapsed meiotic chromosomes. Experimental cell research 316, 158–171. [PubMed: 19686734]

Hanoux V, Pairault C, Bakalska M, Habert R, and Livera G (2007). Caspase-2 involvement during ionizing radiation-induced oocyte death in the mouse ovary. Cell Death Differ 14, 671–681. [PubMed: 17082817]

Harada A, Matsuzaki K, Takeiri A, and Mishima M (2014). The predominant role of apoptosis in gammaH2AX formation induced by aneugens is useful for distinguishing aneugens from clastogens. Mutat Res Genet Toxicol Environ Mutagen 771, 23–29. [PubMed: 25308438]

Humphryes N, and Hochwagen A (2014). A non-sister act: recombination template choice during meiosis. Experimental cell research 329, 53–60. [PubMed: 25158281]

Hunter N (2015). Meiotic Recombination: The Essence of Heredity. Cold Spring Harbor perspectives in biology 7.

Hunter N (2017). Oocyte Quality Control: Causes, Mechanisms, and Consequences. Cold Spring Harb Symp Quant Biol 82, 235–247. [PubMed: 29743337]

Johnston SE, Berenos C, Slate J, and Pemberton JM (2016). Conserved Genetic Architecture Underlying Individual Recombination Rate Variation in a Wild Population of Soay Sheep (Ovis aries). Genetics 203, 583–598. [PubMed: 27029733]

Kadri NK, Harland C, Faux P, Cambisano N, Karim L, Coppieters W, Fritz S, Mullaart E, Baurain D, Boichard D, et al. (2016). Coding and noncoding variants in HFM1, MLH3, MSH4, MSH5, RNF212, and RNF212B affect recombination rate in cattle. Genome research 26, 1323–1332. [PubMed: 27516620]

Kan R, Sun X, Kolas NK, Avdievich E, Kneitz B, Edelmann W, and Cohen PE (2008). Comparative analysis of meiotic progression in female mice bearing mutations in genes of the DNA mismatch repair pathway. Biology of reproduction 78, 462–471. [PubMed: 18057311]

Kerr JB, Myers M, and Anderson RA (2013). The dynamics of the primordial follicle reserve. Reproduction 146, R205–215. [PubMed: 23929903]

Kim DA, and Suh EK (2014). Defying DNA double-strand break-induced death during prophase I meiosis by temporal TAp63alpha phosphorylation regulation in developing mouse oocytes. Molecular and cellular biology 34, 1460–1473. [PubMed: 24515437]

Kim Y, Rosenberg SC, Kugel CL, Kostow N, Rog O, Davydov V, Su TY, Dernburg AF, and Corbett KD (2014). The chromosome axis controls meiotic events through a hierarchical assembly of HORMA domain proteins. Developmental cell 31, 487–502. [PubMed: 25446517]

Kneitz B, Cohen PE, Avdievich E, Zhu L, Kane MF, Hou H, Jr., Kolodner RD, Kucherlapati R, Pollard JW, and Edelmann W (2000). MutS homolog 4 localization to meiotic chromosomes is required for chromosome pairing during meiosis in male and female mice. Genes & development 14, 1085–1097. [PubMed: 10809667]

Kogo H, Tsutsumi M, Inagaki H, Ohye T, Kiyonari H, and Kurahashi H (2012a). HORMAD2 is essential for synapsis surveillance during meiotic prophase via the recruitment of ATR activity. Genes to cells : devoted to molecular & cellular mechanisms 17, 897–912. [PubMed: 23039116]

Kogo H, Tsutsumi M, Ohye T, Inagaki H, Abe T, and Kurahashi H (2012b). HORMAD1-dependent checkpoint/surveillance mechanism eliminates asynaptic oocytes. Genes to cells : devoted to molecular & cellular mechanisms 17, 439–454. [PubMed: 22530760]

Kong A, Thorleifsson G, Stefansson H, Masson G, Helgason A, Gudbjartsson DF, Jonsdottir GM, Gudjonsson SA, Sverrisson S, Thorlacius T, et al. (2008). Sequence variants in the RNF212 gene associate with genome-wide recombination rate. Science 319, 1398–1401. [PubMed: 18239089]

Kouznetsova A, Novak I, Jessberger R, and Hoog C (2005). SYCP2 and SYCP3 are required for cohesin core integrity at diplotene but not for centromere cohesion at the first meiotic division. Journal of cell science 118, 2271–2278. [PubMed: 15870106]

Kouznetsova A, Wang H, Bellani M, Camerini-Otero RD, Jessberger R, and Hoog C (2009). BRCA1-mediated chromatin silencing is limited to oocytes with a small number of asynapsed chromosomes. Journal of cell science 122, 2446–2452. [PubMed: 19531582]

Lao JP, and Hunter N (2010). Trying to avoid your sister. PLoS biology 8, e1000519. [PubMed: 20976046]

Li X, and Schimenti JC (2007). Mouse pachytene checkpoint 2 (trip13) is required for completing meiotic recombination but not synapsis. PLoS genetics 3, e130. [PubMed: 17696610]

Livera G, Petre-Lazar B, Guerquin MJ, Trautmann E, Coffigny H, and Habert R (2008). p63 null mutation protects mouse oocytes from radio-induced apoptosis. Reproduction 135, 3–12. [PubMed: 18159078]

Lynn A, Soucek R, and Borner GV (2007). ZMM proteins during meiosis: Crossover artists at work. Chromosome Res 15, 591–605. [PubMed: 17674148]

Mahadevaiah SK, Turner JM, Baudat F, Rogakou EP, de Boer P, Blanco-Rodriguez J, Jasin M, Keeney S, Bonner WM, and Burgoyne PS (2001). Recombinational DNA double-strand breaks in mice precede synapsis. Nature genetics 27, 271–276. [PubMed: 11242108]

Malki S, van der Heijden GW, O'Donnell KA, Martin SL, and Bortvin A (2014). A role for retrotransposon LINE-1 in fetal oocyte attrition in mice. Developmental cell 29, 521–533. [PubMed: 24882376]

Niu H, Wan L, Baumgartner B, Schaefer D, Loidl J, and Hollingsworth NM (2005). Partner choice during meiosis is regulated by Hop1-promoted dimerization of Mek1. Molecular biology of the cell 16, 5804–5818. [PubMed: 16221890]

Prugar E, Burnett C, Chen X, and Hollingsworth NM (2017). Coordination of Double Strand Break Repair and Meiotic Progression in Yeast by a Mek1-Ndt80 Negative Feedback Loop. Genetics 206, 497–512. [PubMed: 28249986]

Qiao H, Prasada Rao HB, Yang Y, Fong JH, Cloutier JM, Deacon DC, Nagel KE, Swartz RK, Strong E, Holloway JK, et al. (2014). Antagonistic roles of ubiquitin ligase HEI10 and SUMO ligase RNF212 regulate meiotic recombination. Nature genetics 46, 194–199. [PubMed: 24390283]

Rao HB, Qiao H, Bhatt SK, Bailey LR, Tran HD, Bourne SL, Qiu W, Deshpande A, Sharma AN, Beebout CJ, et al. (2017). A SUMO-ubiquitin relay recruits proteasomes to chromosome axes to regulate meiotic recombination. Science 355, 403–407. [PubMed: 28059716]

Reynolds A, Qiao H, Yang Y, Chen JK, Jackson N, Biswas K, Holloway JK, Baudat F, de Massy B, Wang J, et al. (2013). RNF212 is a dosage-sensitive regulator of crossing-over during mammalian meiosis. Nature genetics 45, 269–278. [PubMed: 23396135]

Ribeiro J, Abby E, Livera G, and Martini E (2016). RPA homologs and ssDNA processing during meiotic recombination. Chromosoma 125, 265–276. [PubMed: 26520106]

Rinaldi VD, Bolcun-Filas E, Kogo H, Kurahashi H, and Schimenti JC (2017). The DNA Damage Checkpoint Eliminates Mouse Oocytes with Chromosome Synapsis Failure. Molecular cell 67, 1026–1036 e1022. [PubMed: 28844861]

Roig I, Dowdle JA, Toth A, de Rooij DG, Jasin M, and Keeney S (2010). Mouse TRIP13/PCH2 is required for recombination and normal higher-order chromosome structure during meiosis. PLoS genetics 6.

Rosenberg SC, and Corbett KD (2015). The multifaceted roles of the HORMA domain in cellular signaling. The Journal of cell biology 211, 745–755. [PubMed: 26598612]

Royo H, Prosser H, Ruzankina Y, Mahadevaiah SK, Cloutier JM, Baumann M, Fukuda T, Hoog C, Toth A, de Rooij DG, et al. (2013). ATR acts stage specifically to regulate multiple aspects of mammalian meiotic silencing. Genes & development 27, 1484–1494. [PubMed: 23824539]

Shin YH, Choi Y, Erdin SU, Yatsenko SA, Kloc M, Yang F, Wang PJ, Meistrich ML, and Rajkovic A (2010). Hormad1 mutation disrupts synaptonemal complex formation, recombination, and

chromosome segregation in mammalian meiosis. PLoS genetics 6, e1001190. [PubMed: 21079677]

Shin YH, McGuire MM, and Rajkovic A (2013). Mouse HORMAD1 is a meiosis i checkpoint protein that modulates DNA double- strand break repair during female meiosis. Biology of reproduction 89, 29. [PubMed: 23759310]

Stanzione M, Baumann M, Papanikos F, Dereli I, Lange J, Ramlal A, Trankner D, Shibuya H, de Massy B, Watanabe Y, et al. (2016). Meiotic DNA break formation requires the unsynapsed chromosome axis-binding protein IHO1 (CCDC36) in mice. Nature cell biology 18, 1208–1220. [PubMed: 27723721]

Suh EK, Yang A, Kettenbach A, Bamberger C, Michaelis AH, Zhu Z, Elvin JA, Bronson RT, Crum CP, and McKeon F (2006). p63 protects the female germ line during meiotic arrest. Nature 444, 624–628. [PubMed: 17122775]

Sun X, and Cohen PE (2013). Studying recombination in mouse oocytes. Methods in molecular biology 957, 1–18. [PubMed: 23138941]

Turner JM, Mahadevaiah SK, Fernandez-Capetillo O, Nussenzweig A, Xu X, Deng CX, and Burgoyne PS (2005). Silencing of unsynapsed meiotic chromosomes in the mouse. Nature genetics 37, 41–47. [PubMed: 15580272]

Vader G, and Musacchio A (2014). HORMA domains at the heart of meiotic chromosome dynamics. Developmental cell 31, 389–391. [PubMed: 25458007]

Wojtasz L, Cloutier JM, Baumann M, Daniel K, Varga J, Fu J, Anastassiadis K, Stewart AF, Remenyi A, Turner JM, et al. (2012). Meiotic DNA double-strand breaks and chromosome asynapsis in mice are monitored by distinct HORMAD2-independent and - dependent mechanisms. Genes & development 26, 958–973. [PubMed: 22549958]

Wojtasz L, Daniel K, Roig I, Bolcun-Filas E, Xu H, Boonsanay V, Eckmann CR, Cooke HJ, Jasin M, Keeney S, et al. (2009). Mouse HORMAD1 and HORMAD2, two conserved meiotic chromosomal proteins, are depleted from synapsed chromosome axes with the help of TRIP13 AAA-ATPase. PLoS genetics 5, e1000702. [PubMed: 19851446]

Ye Q, Kim DH, Dereli I, Rosenberg SC, Hagemann G, Herzog F, Toth A, Cleveland DW, and Corbett KD (2017). The AAA+ ATPase TRIP13 remodels HORMA domains through N-terminal engagement and unfolding. The EMBO journal 36, 2419–2434. [PubMed: 28659378]

Yun Y, Holt JE, Lane SI, McLaughlin EA, Merriman JA, and Jones KT (2014). Reduced ability to recover from spindle disruption and loss of kinetochore spindle assembly checkpoint proteins in oocytes from aged mice. Cell cycle 13, 1938–1947. [PubMed: 24758999]

Highlights

- RNF212, a SUMO ligase required for crossovers, also mediates oocyte quality control
- RNF212 promotes apoptosis of oocytes that experienced defects in meiotic prophase I
- RNF212 works with HORMAD1 to impede repair of residual DSBs as chromosomes desynapse
- Impeded DSBs signal that meiosis was defective and trigger oocyte apoptosis

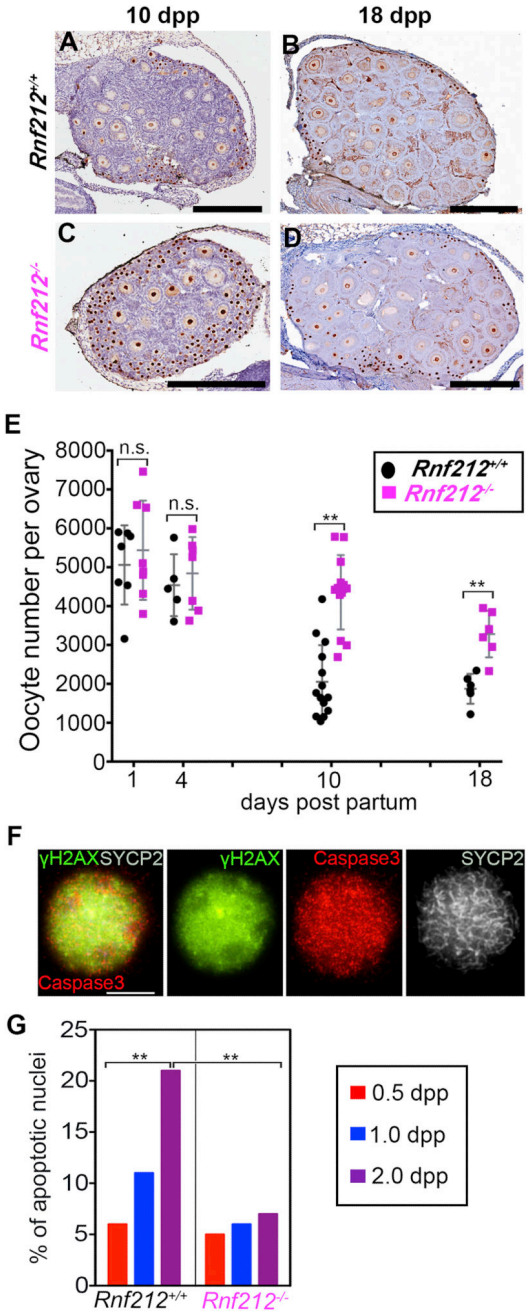

Figure. 1. RNF212 promotes postnatal oocyte apoptosis

(**A**, **B**) Representative wild type and (**C**, **D**) *Rnf212* mutant ovary sections from 10 and 18 dpp females immunostained for p63 with hematoxylin counterstaining. (**E**) Oocyte counts in wild type and *Rnf212*−/− mutant ovaries. For immunofluorescence-stained ovary sections (1 and 4 dpp counts), MVH/SYCP3-positive cells with or without p63 staining-positive nuclei were counted. For immunohistochemistry-stained sections (10 and 18 dpp counts), p63-positive oocyte nuclei with characteristic surrounding granulosa cell layers were counted. In both cases, counts were made for every fifth section and multiplied to calculate the total number of oocytes per ovary, as described (Di Giacomo et al., 2005). For each genotype, 6-9

ovaries from 3-5 mice were analyzed. Error bars show mean ± Sd. $^{**}P \leq 0.01$, two-tailed Mann-Whitney test. (**F**) Representative wild-type oocyte nucleus at 2 dpp immunostained for γH2AX (green), caspase 3 (red) and chromosome axis marker SYCP2 (grey). (**G**) Quantification of apoptotic nuclei at successive days postpartum. For each data point, 96-109 nuclei were counted from two animals. $^{**}P < 0.01$, *z*-test. Scale bar in F. is 10μm.

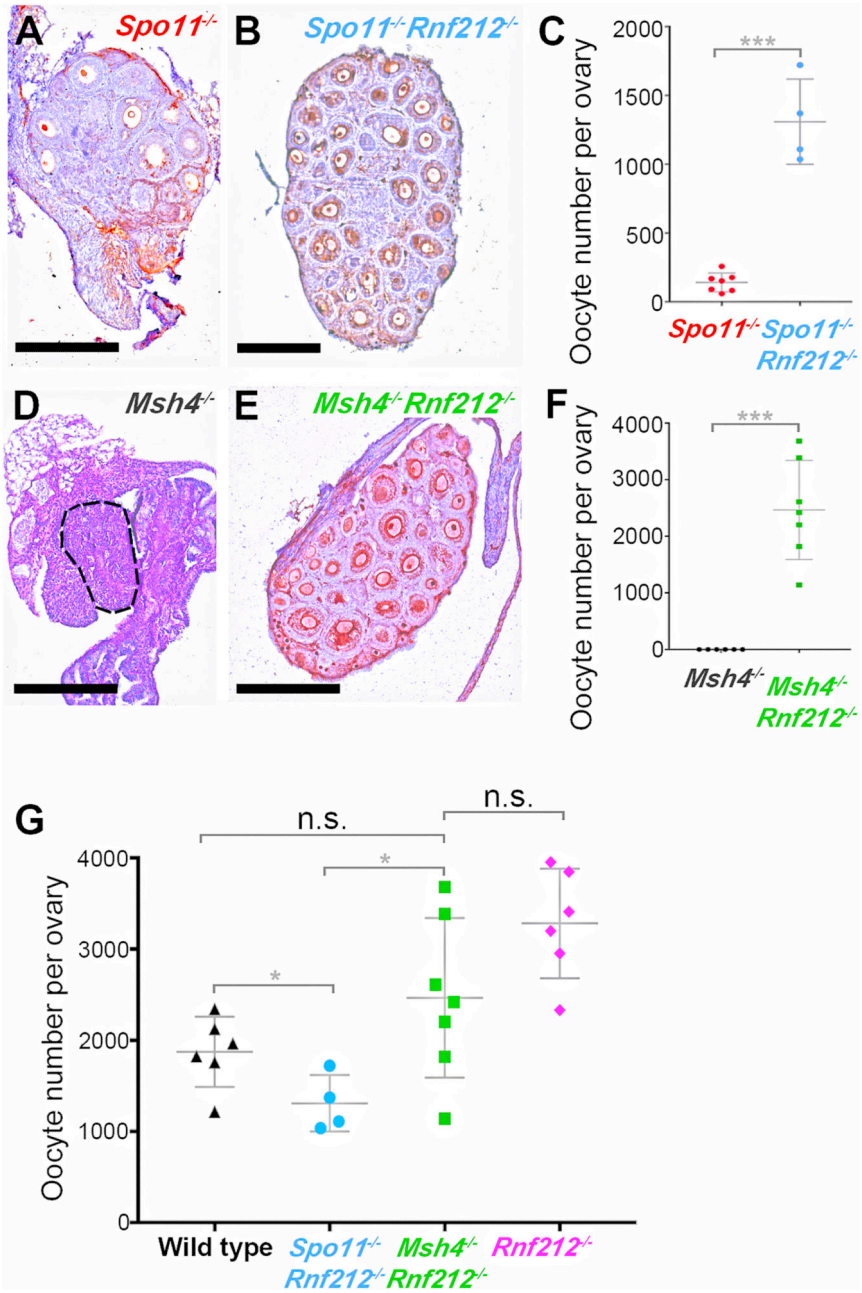

Figure 2. RNF212 is required for wholesale oocyte apoptosis in response to defects in early meiotic prophase.

(**A**) Representative *Spo11*$^{-/-}$ and (**B**) *Spo11*$^{-/-}$ *Rnf212*$^{-/-}$ 18 dpp ovary sections immunostained for p63 with hematoxylin counterstaining. (**C**) Oocyte counts in *Spo11*$^{-/-}$ and *Spo11*$^{-/-}$ *Rnf212*$^{-/-}$ ovaries at 18 dpp. (**D**) Representative *Msh4*$^{-/-}$ and (**E**) *Rnf212*$^{-/-}$ *Msh4*$^{-/-}$ 18 dpp ovary sections. The dashed line highlights the degenerate ovary in the *Msh4*$^{-/-}$ mutant. (**F**) Oocyte counts at 18 dpp. (**G**) Oocyte counts at 18 dpp in wild type, *Rnf212*$^{-/-}$, *Spo11*$^{-/-}$ *Rnf212*$^{-/-}$, and *Msh4*$^{-/-}$ *Rnf212*$^{-/-}$. ***$P \leq 0.001$, two-tailed Mann-Whitney test. Error bars show mean ± SD. Scale bars for ovary sections are 300 μm.

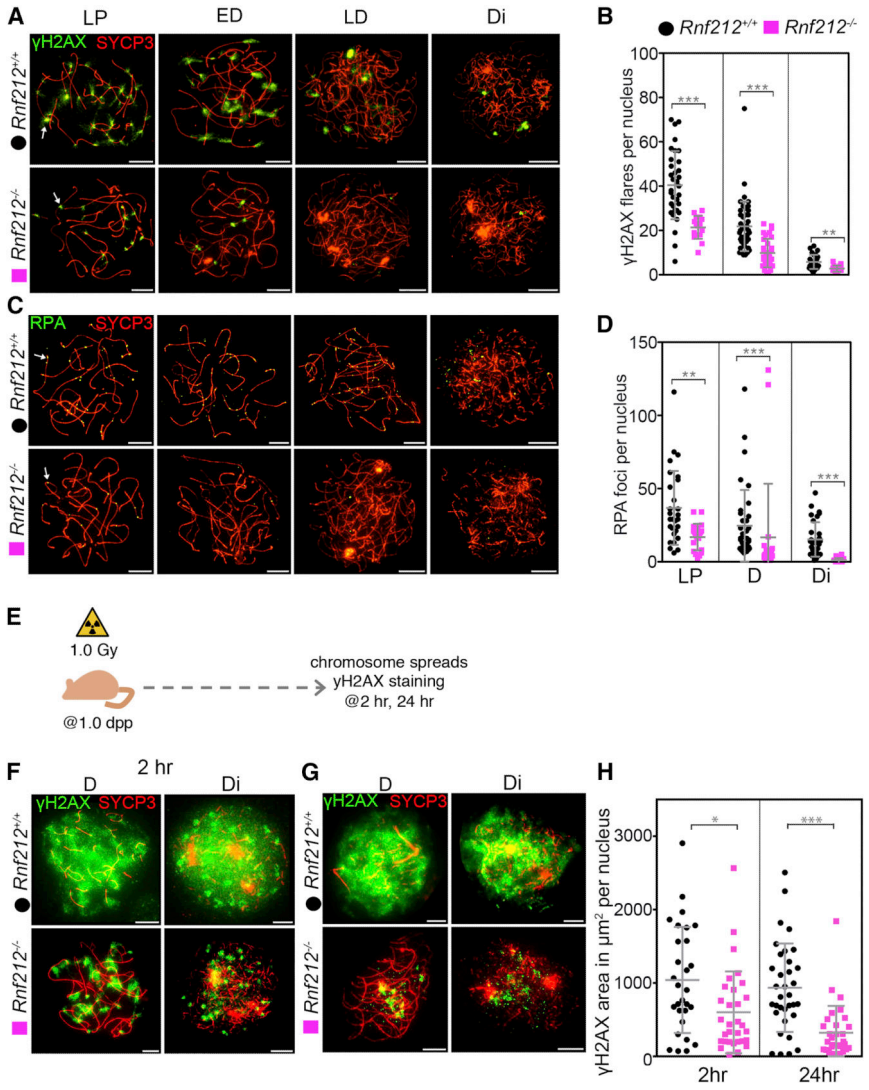

Figure. 3. RNF212 impedes DNA-damage repair in early-postnatal oocytes.

(**A**) Representative 1 dpp oocyte nuclei at the indicated stages immunostained for chromosome axis marker SYCP3 (red) and γH2AX (green). Arrow indicates an individual γH2AX flare. (**B**) Quantification of γH2AX flares in oocyte nuclei at successive prophase substages. All counts are for 20-40 nuclei from two independent animals. (**C**) Representative 1 dpp oocyte nuclei at the indicated stages immunostained for chromosome axis marker SYCP3 (red) and RPA (green). Arrows highlight individual RPA foci. (**D**) Quantification of RPA foci in 1 dpp oocyte nuclei at successive prophase substages. All counts are for 20-35 nuclei from two independent animals. (**E**) Experimental regimen to monitor the acute response to irradiation-induced DNA damage. (**F**) Representative oocyte nuclei 2 hrs after irradiation immunostained for chromosome SYCP3 (red) and γH2AX (green). (**G**) Representative oocyte nuclei 24 hrs after irradiation. (**H**) Quantification of γH2AX immunostaining areas in oocyte nuclei at indicated times after irradiation. All counts are for 20-25 nuclei from two independent animals. LP, late pachynema; ED, early diplonema; LD,

late diplonema; Di, early dictyotene. $^{**}P \leq 0.01$, $^{***}P \leq 0.001$, two-tailed Mann-Whitney test. Error bars show mean ± SD. Scale bars, 10μm.

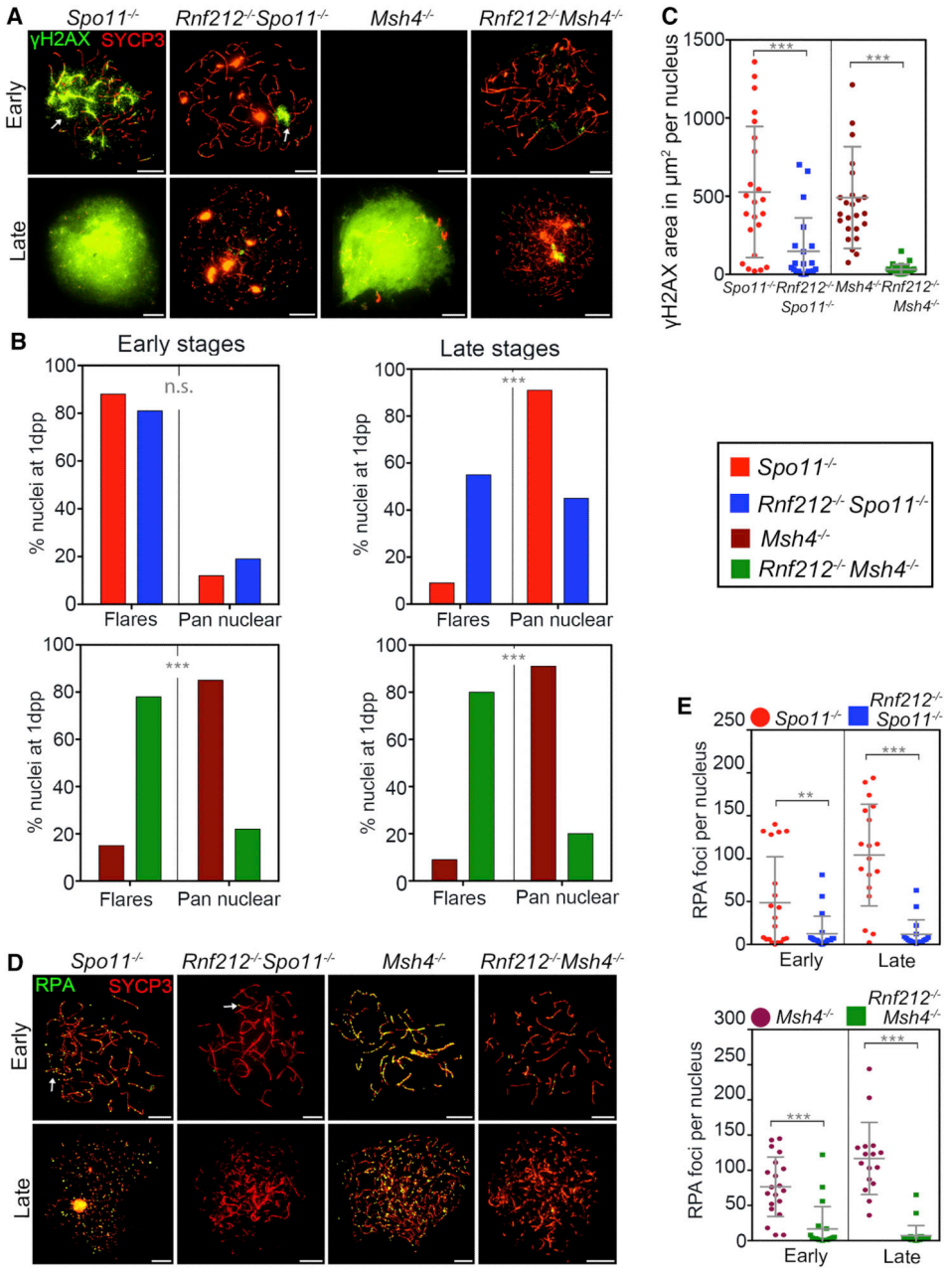

Figure. 4. RNF212 impedes DNA-damage repair in *Spo11* and *Msh4* mutants.

(**A**) Representative 1 dpp oocyte nuclei from the indicated strains immunostained for chromosome axis marker SYCP3 (red) and γH2AX (green). (**B**) Quantification of γH2AX flares and pan nuclear γH2AX staining in 1 dpp oocytes. All counts are for 90-110 nuclei from two independent animals. (**C**) Quantification of γH2AX immunostaining areas in 1 dpp oocytes. All counts are for 20-30 nuclei from two independent animals. (**D**) Representative 1 dpp oocyte nuclei from the indicated strains immunostained for chromosome axis marker SYCP3 (red) and RPA (green). Arrows highlight individual RPA foci. (**E**) Quantification of RPA foci in 1 dpp oocytes from the indicated strains. All counts are for 20-30 nuclei from two independent animals. χ^2 contingency test was used for

analysis of data in (**B**); two-tailed Mann-Whitney test for (**C**) and (**E**). n.s. not significant (P=0.17), ** $P \leq 0.01$, *** $P \leq 0.001$. Error bars show means ± SD. Scale bars, 10μm.

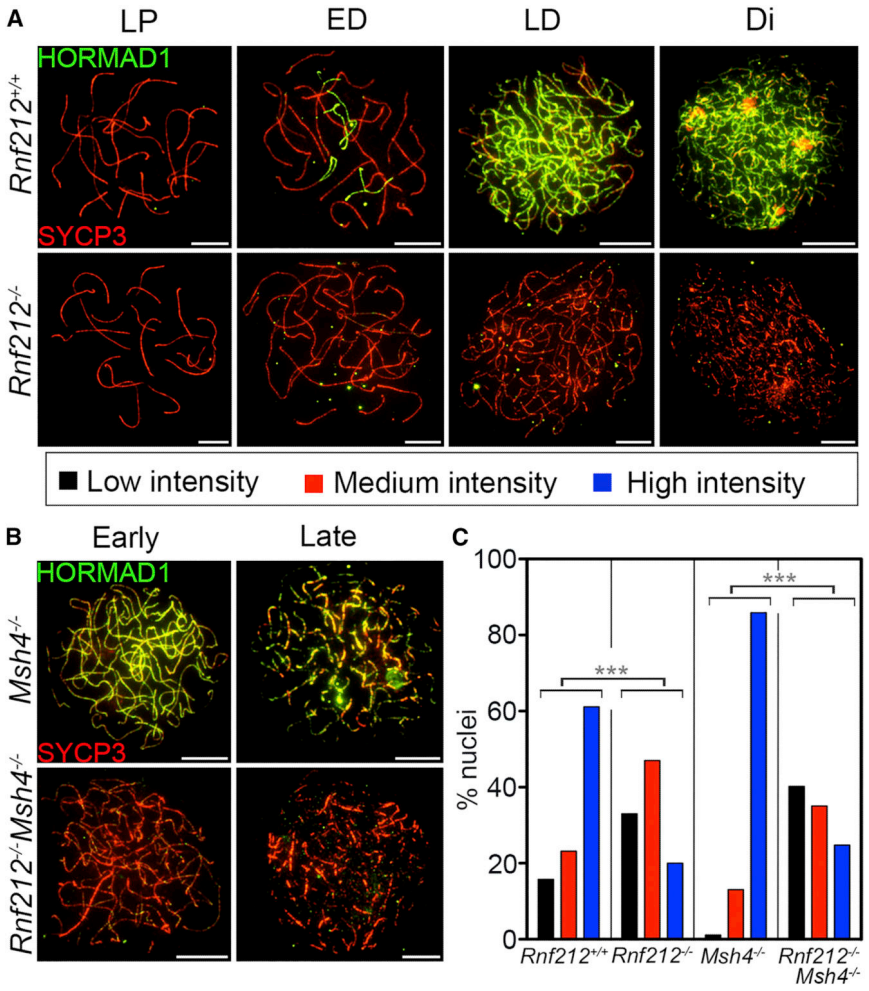

Fig. 5. RNF212 promotes association of HORMAD1 with desynapsed homolog axes.

(**A**, **B**) Representative 1 dpp oocyte nuclei from the indicated strains immunostained for SYCP3 (red) and HORMAD1 (green). LP, late pachynema; ED, early diplonema; LD, late diplonema; Di, early dictyotene. (**C**) Quantification of HORMAD1 signal intensity ratios in the indicated strains. All counts are for 80-110 nuclei from two independent animals. For each nucleus, total signal for HORMAD1 was divided by total signal for SYCP3: ratio of ≤0.2, low intensity; 0.21-0.4, medium intensity; ≥0.41, high intensity (Figure S5). ***$P <$ 0.001, *G*-test. Scale bars, 10μm.

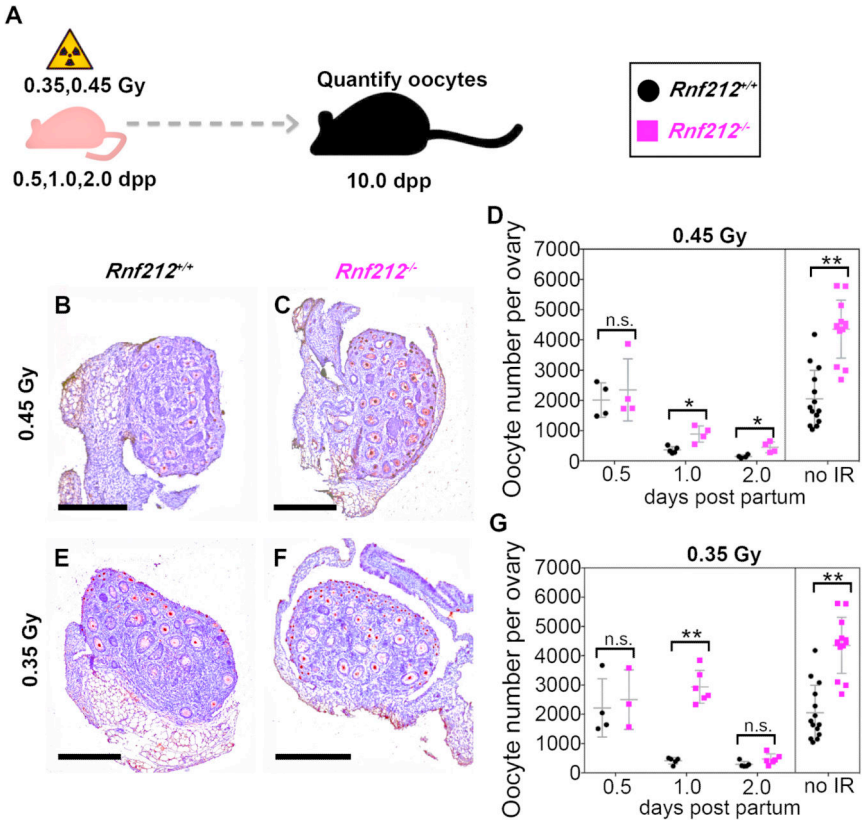

Figure. 6. RNF212 sensitizes early-postnatal oocytes to radiation-induced apoptosis.

(**A**) Experimental regimen for irradiation experiments. (**B**, **C** and **E**, **F**) 10 dpp ovary sections from *Rnf212*$^{+/+}$ and *Rnf212*$^{-/-}$ females following irradiation with 0.45 or 0.35 Gy at 1 dpp. (**D** and **G**) Oocyte counts following irradiation with 0.45 or 0.35 Gy, respectively. Error bars show means ± SD. *$P \leq 0.05$, **$P \leq 0.01$, ***$P \leq 0.001$, two-tailed Mann-Whitney test. Scale bars, 300 μm.

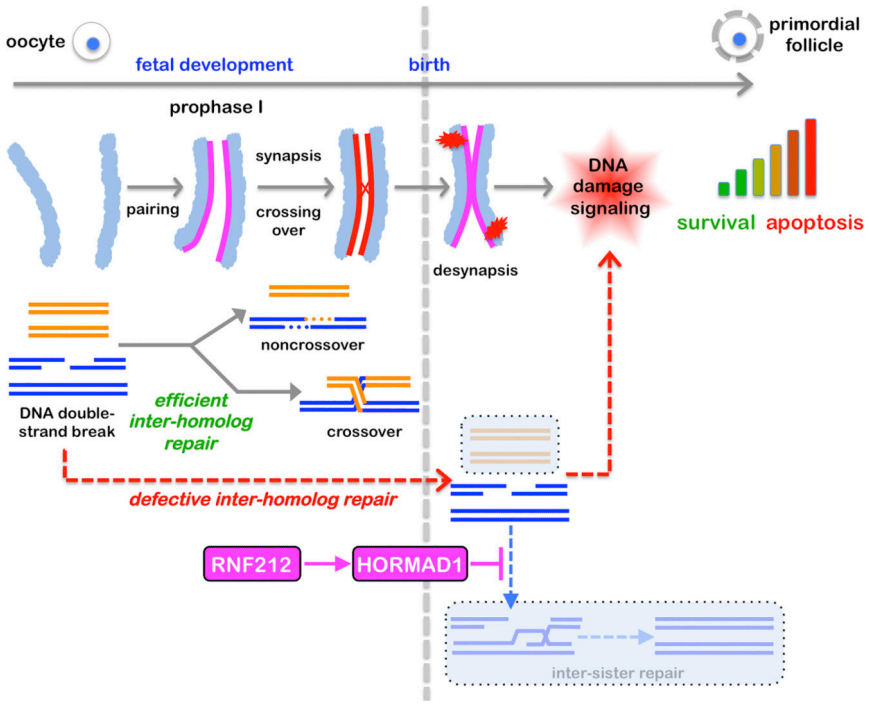

Figure. 7. Logic of pre-follicle oocyte quality control.

Timeline of chromosomal and DNA events during oocyte meiotic prophase. Magenta lines indicate homolog axes associated with HORMAD1. Red “explosions” represent unrepaired DSBs. Transparent boxes indicate repair pathways that are unavailable following desynapsis in diplotene. Inter-sister repair is actively impeded by RNF212-dependent reassociation of HORMAD1 with desynapsed homolog axes. Consequently, residual DSBs persist and robustly signal via the DNA-damage response pathway. The integrated level of damage signaling from all residual DSBs dictates whether an individual oocyte undergoes apoptosis or survives to form a primordial follicle and become established in the ovarian reserve.

KEY RESOURCE TABLE

Antibodies		
mouse anti-p63	Santa Cruz Biotechnology	sc-25268
rabbit anti-MVH	Abcam	ab13840
rabbit anti-SYCP3	Santa Cruz Biotechnology	sc-33195
anti-rabbit 488	Molecular Probes	A11070
anti-mouse 594	Molecular Probes	A11020
anti-rabbit 568	Molecular Probes	A11036
anti-mouse 488	Molecular Probes	A11029
Biotin-conjugated anti-mouse secondary antibody	ThermoFisher Scientific	A16076
human anti-centromere antibodies	ImmunoVision	ACA; HCT-0100
anti-human 555 secondary antibody	Molecular Probes	A-21433
mouse anti-SYCP3	Santa Cruz Biotechnology	sc-74568
guinea pig anti-SYCP2	a gift from Christer Höög	N/A
rabbit monoclonal anti-RPA32	Abcam	ab76420
rabbit anti-REC8	a gift from Scott Keeney	N/A
mouse monoclonal anti-γH2AX	Millipore	05-636
rabbit polyclonal anti-γH2AX	Bethyl laboratories	A300-081A
goat polyclonal anti-Caspase3 (L-18)	Santa Cruz Biotechnology	Sc-1225
rabbit anti-HORMAD1	a gift from Attila Toth	N/A
anti-mouse 555	Molecular Probes	A21425
anti-guinea pig fluorescein isothiocyanate	Jackson Labs	106-096-006 FITC

Chemicals, Peptides, and Recombinant Proteins		
Protein Block, Serum Free, Blocking, Unconjugated, Liquid form, Immunohistochemistry, 110 mL	Agilent Dako	X090930-2
ABC-DAB Peroxidase system	Vector Laboratories	Cat# PK-6100
Tyrode’s Solution, Acidic	Sigma-Aldrich	Cat# T1788
milrnone	Sigma-Aldrich	Cat# 78415-72-2
3% BSA	Thermo Fisher Scientific	Cat# AM2616
ProLong Gold antifade reagent (Molecular Probes)	Thermo Fisher Scientific	Cat# P36930
M2 medium	Sigma-Aldrich	Cat# M7167

REAGENT or RESOURCE	SOURCE	IDENTIFIER
Software and Algorithms		
Volocity 6.3	Perkin Elmer	N/A
Aperio ImageScope software	Leica	N/A